Supplementary Information (SI) for Energy & Environmental Science.

Customizing vertical electrodeposition orientation and interfacial solvation to enable magnesium metal anodes with ultrahigh areal capacity

Guyue Li [a, b, c], Liu Cao [a, c], Meng Lei [a, b, c], Keyi Chen [a, c], Chilin Li [a, b, c, *]

[a] State Key Laboratory of High Performance Ceramics and Superfine Microstructure, Shanghai Institute of Ceramics, Chinese Academy of Sciences, 585 He Shuo Road, Shanghai 201899, China. Email: chilinli@mail.sic.ac.cn

[b] Center of Materials Science and Optoelectronics Engineering, University of Chinese Academy of Sciences, Beijing 100049, China.

[c] CAS Key Laboratory of Materials for Energy Conversion, Shanghai Institute of Ceramics, Chinese Academy of Sciences, Shanghai 201899, China.

Experimental Section

Electrolyte preparation

The $Mg(TFSI)_2$-BrFB-G2 electrolyte (denoted as MBG) was prepared in an argon-filled glovebox (with oxygen content <0.5 ppm and H_2O content <0.5 ppm). Firstly, the 3-bromofluorobenzene (BrFB, GR, 99% purity, Adamas) additive with predetermined amount (10 μL, 20 μL, 50 μL or 100 μL) was added into the diethylene glycol dimethyl ether (G2, 99.5%, Aladdin) solvent, which was then stirred for at least 12 h to form a solution with magnesium bis(trifluoromethylsulfonyl)imide ($Mg(TFSI)_2$, 99.5%, Dodo Chem) salt concentration of 0.25 M. If without the addition of BrFB additive, the corresponding electrolyte is abbreviated as MG. Other electrolytes were also prepared by replacing BrFB with bromobenzene (BrB, GR, Adamas), fluorobenzene (FB, 99%, Aladdin), 1,3-dibromobenzene (BrBrB, GR, Adamas) and 1,3-difluorobenzene (FFB, GR, Adamas).

Electrode preparation

Mg anode preparation Mg foils (99.9%, 0.1 mm thick) were purchased from Hefei KE JING Materials Technology co., LTD. Then the Mg foils were cut into the disks with a diameter of 10 mm and polished with a scalpel in an argon-filled glovebox (with oxygen content <0.5 ppm and H_2O content <0.5 ppm) to remove oxide layer.

CuS cathode preparation CuS was prepared according to the published work.[1] To prepare the CuS cathode slurry, the as-prepared CuS, Super P carbon black and poly (vinyl difluoride) (PVDF, Sigma Aldrich) were thoroughly mixed together in a weight ratio of 7:2:1 in N-methyl-2-pyrrolidone (NMP, AR, Sinopharm Chemical Reagent Co.) solvent by grinding in an agate mortar. The slurry was coated on the 8-mm-diameter carbon paper (Toray, TGP-H-060) and dried at 60 °C in the vacuum oven for 12 h. The areal loading of CuS active material is around 1.0 mg cm^{-2}.

Electrochemical measurements

To obtain the electrochemical performance on LAND battery testing system (CTA2001A), Mg||Mg symmetric cells, carbon-coated-Al||Mg asymmetric cells and CuS||Mg full cells were assembled by using CR2032-type coin cells, with the 19-mm-diameter separator (GF, Whatman) and 30 μL predetermined electrolyte. Electrochemical impedance spectroscopy (EIS) was performed from 10 MHz to 0.1 Hz in a temperature range of 30~50 °C by the Solartron Frequency Analyzer. Linear sweep voltammetry (LSV) was carried out based on the asymmetric cells with stainless steel/nickel/copper disks as working electrodes at a scan rate of 1 mV s^{-1}. Cyclic voltammetry (CV) measurement based on symmetric cells (from -1.0 V to 1.0 V vs. Mg/Mg^{2+}), asymmetric cells (from -0.5 V to 1.5 V vs. Mg/Mg^{2+}) and full cells (from 0.2 V to 2.6 V vs. Mg/Mg^{2+}) was conducted using Versa STAT3 work station at a scan rate of 0.1 mV s^{-1}. Tafel curves based on symmetric cells were obtained from -100 mV to 100 mV at a scan rate of 0.1 mV s^{-1}. And the corresponding exchange current density was calculated by Butler-Volmer Equation.

The Mg^{2+} transport number (t_{Mg2+}) was also measured on VersaSTAT3 workstation using the Mg||Mg cell architecture with a DC polarization voltage of 10 mV. The t_{Mg2+} value could be obtained according to the following equation:

$$t_{Mg} = \frac{I_{SS}(\Delta V - I_0 R_0)}{I_0(\Delta V - I_{SS} R_{SS})}$$

where ΔV is 10 mV, I_0 and I_{ss} are the currents at initial and steady states, R_0 and R_{ss} are the corresponding resistances before and after polarization process.

All the cells were assembled in an argon-filled glovebox (with oxygen content <0.5 ppm and H_2O content <0.5 ppm).

Material characterizations

X-ray diffraction (XRD) characterization was measured by Bruker D8 Discover diffractometer with Cu-K_α radiation. The preparation of deposited Mg for XRD is based on the configuration of c-Al||Mg asymmetric cell. After the 20 mAh cm^{-2}-deposition of Mg on c-Al foil, the deposited Mg can be easily stripped with a scalpel for XRD testing.

The morphology images and energy dispersive X-ray spectrometer (EDS) elemental mapping were obtained by a field-emission scanning electron microscopy (SEM, HITACHI SU8220). Further information of microstructure and spatial distribution of components in ASEI were disclosed by transmission electron microscopy (TEM) images and selected area electron diffraction (SAED) patterns collected from JEOL JSM-6700F, operated with an acceleration voltage of 200 kV. X-ray photoelectron spectroscopy (XPS, ESCAlab-250, Thermo Fisher Scientific) was used to perform the anodic interface composition. Raman spectra of BrFB, G2 $Mg(TFSI)_2$-G2 (MG), BrFB-G2 (BG) and $Mg(TFSI)_2$-BrFB-G2 (MBG) electrolytes were collected with DXR Raman Microscope (Thermal Scientific Corporation, USA) using the 532 nm He-Ne laser source. BrFB, G2 and BG electrolytes were used for nuclear magnetic resonance (NMR) spectroscopy measurement by Bruker Avance spectrometer. Before characterizations, the samples after cycling were carefully washed with G2 to remove the residual electrolyte and dried thoroughly in an argon-filled glovebox (with oxygen content <0.5 ppm and H_2O content <0.5 ppm).

DFT calculation

Quantum chemistry calculation was carried out with the Gaussian 09W software package. The molecule structure optimization was performed with the M06-2X/def2-TZVP level, and the molecular orbital energy and binding energy are calculated at the M06-2X/def2-TZVPP level based on the optimized geometries. The ESP mapping was acquired by the further calculation based on Gaussian check files.

Geometry optimizations were further performed using DFT with the Perdew-Burke-Ernzerhof (PBE) exchange-correlation functional implemented in Vienna Ab-initio Simulation Package.[2,3] The projector augmented wave (PAW) method was used to describe the core-valence interactions. The kinetic energy cutoff for the plane-wave expansion is set at 450 eV. A $1\times1\times1$ Gamma sampling k-point grid is used for the slabs. The bottom two layers of atoms in the slabs are frozen and the lattices are kept fixed at the optimized bulk values, and the rest of atoms are fully relaxed during optimization.

The threshold of total energy and absolute value of force acting on each atom are set at 1×10^{-6} eV and 2×10^{-2} eV Å^{-1}, respectively. A vacuum layer of 10 Å and dipole correction are applied for the slabs. The DFT-D3 method is applied to correct the dispersion interaction.[4] The adsorption energy (E_a) is calculated using the equation: $E_a = E_{slab+A} - E_{slab} - E_A$, where E_{slab+A}, E_{slab} and E_A are the total energies of adsorbed slab, pristine slab and adsorbate species, respectively.

Climbing image nudged elastic band (CINEB) method is applied to calculate the Mg migration barrier in bulk structure.[5] For bulk MgO, $MgBr_2$ and MgF_2, the Mg hopping step is calculated between one Mg atom and its nearest site along the lowest energy migration path. The start-point and end-point structures are relaxed prior to the CINEB calculation. The intermediate states with a spring constant of 5.0 eV Å^{-2} are applied between start and end states. All atoms are relaxed and the lattices are fixed during calculation. The force convergent criterion for CINEB calculation is set at 3×10^{-2} eV Å^{-1}.

The molecular dynamics (MD) calculations were carried out using the Forcite package. Firstly, amorphous cell is used to build the model and conduct preliminary structural optimization with the density of 1.1 g cm^{-3}. The initial structures of MG and MBG systems are set up by randomly placing numbers of Mg^{2+}, TFSI^{-}, BrFB and G2 based on experimental densities and molar ratios. The bond and non-bond parameters of molecules and ions are obtained from COMPASS II force field. The equilibration in NVT ensemble was performed for 1000 ps with an interval of 1 fs and the whole simulation is maintained at a temperature of 298 K. In addition, the Mg^{2+} diffusion coefficient (D_{Mg2+}) in electrolyte is calculated using the Einstein relation:

$$D_{Mg2+} = \lim_{t\to\infty} \frac{\langle MSD(t) \rangle}{6t}$$

where the average mean-square displacement (MSD(t)) represents the mean-square displacement of a molecule center of mass and t denotes time; $\langle\rangle$ denotes an ensemble average.

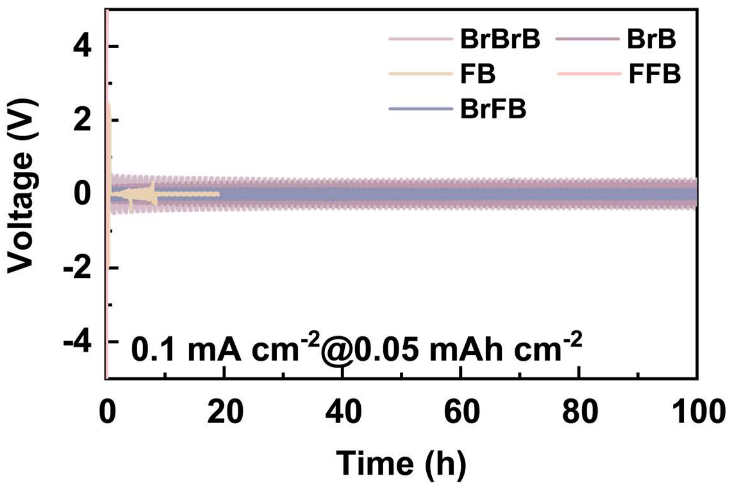

Figure S1. Voltage profiles of Mg||Mg symmetric cells in MG based electrolytes with different additives at 0.1 mA cm^{-2}@0.05 mAh cm^{-2}.

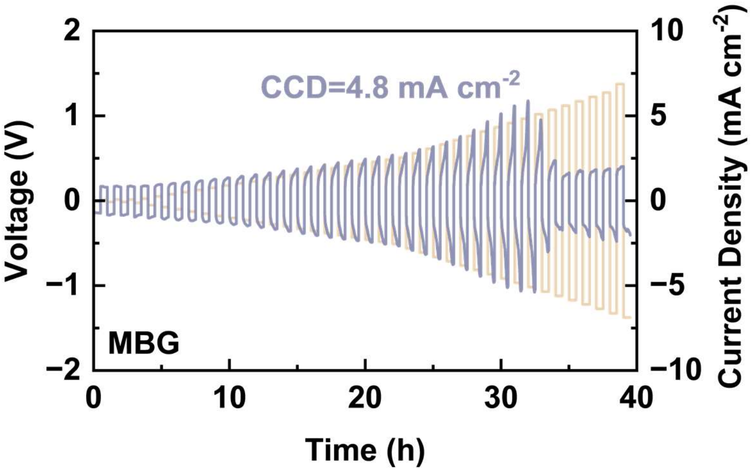

Figure S2. CCD measurement of Mg||Mg symmetric cell in MBG electrolyte.

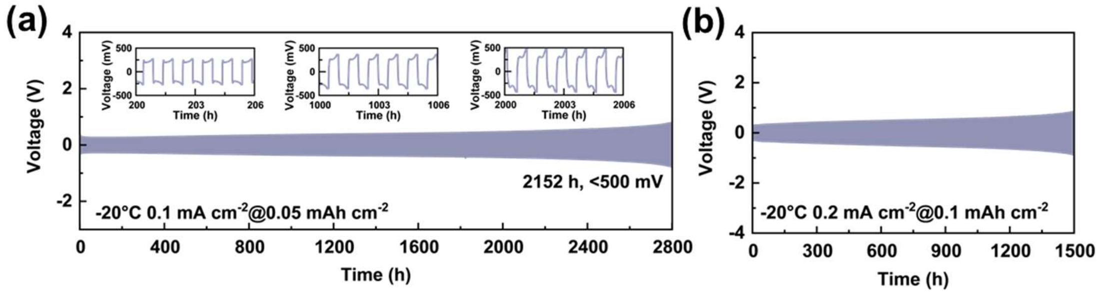

Figure S3. Low-temperature voltage profiles of Mg||Mg symmetric cells in MBG electrolyte at (a) 0.1 mA cm^{-2}@0.05 mAh cm^{-2} and (b) 0.2 mA cm^{-2}@0.1 mAh cm^{-2}.

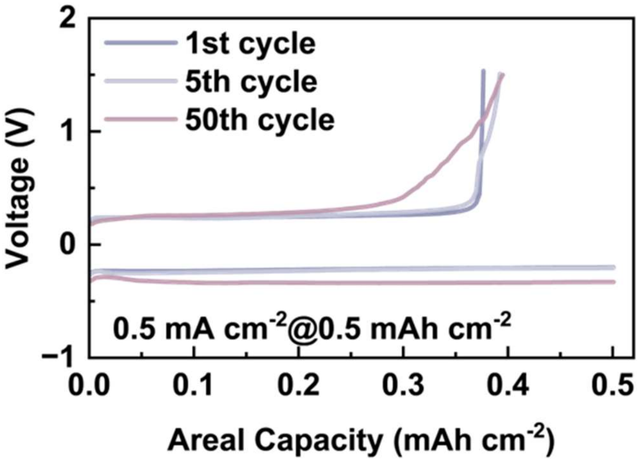

Figure S4. Voltage profiles of Mg plating/stripping of c-Al||Mg asymmetric cell in MBG electrolyte with 0.25 M $Mg(TFSI)_2$ at different cycling stages.

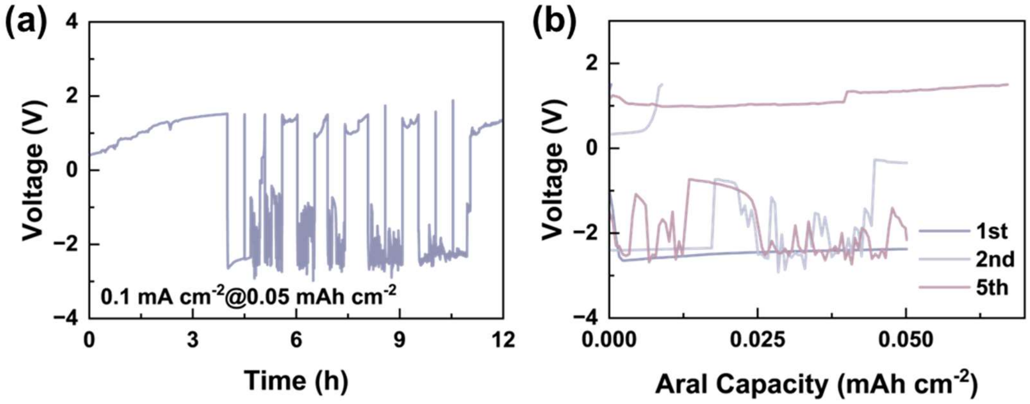

Figure S5. (a-b) Voltage profiles of Mg plating/stripping of c-Al||Mg asymmetric cell in MG electrolyte.

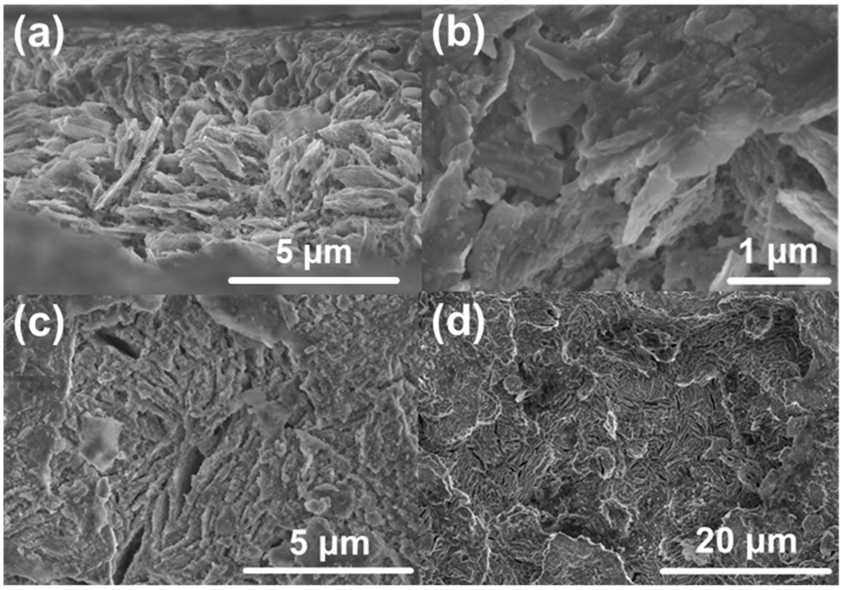

Figure S6. (a-b) Cross-section SEM images of Mg electrode after plating at an areal capacity of 0.05 mAh cm^{-2}. (c) Surface SEM image of Mg electrode after stripping at an areal capacity of 0.05 mAh cm^{-2}. (d) Surface SEM image of Mg electrode after plating at an areal capacity of 0.05 mAh cm^{-2}.

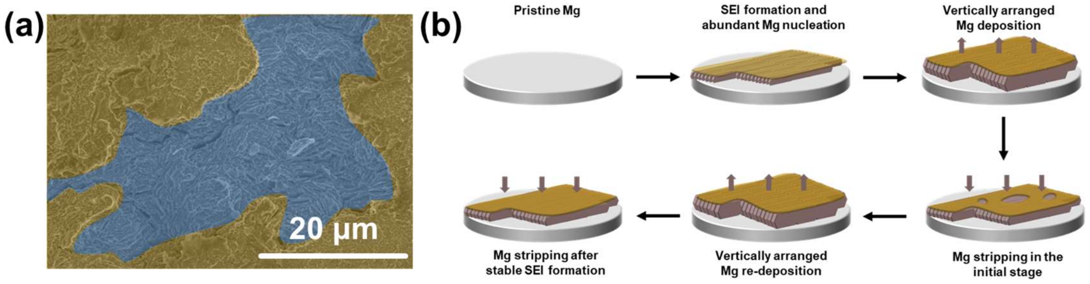

Figure S7. (a) Top-view SEM image of Mg electrode with coloring to distinguish SEI and un-stripped Mg deposition after stripping at an areal capacity of 0.05 mAh cm^{-2}. (b) Schematic illustration of SEI evolution and Mg plating/stripping behaviors.

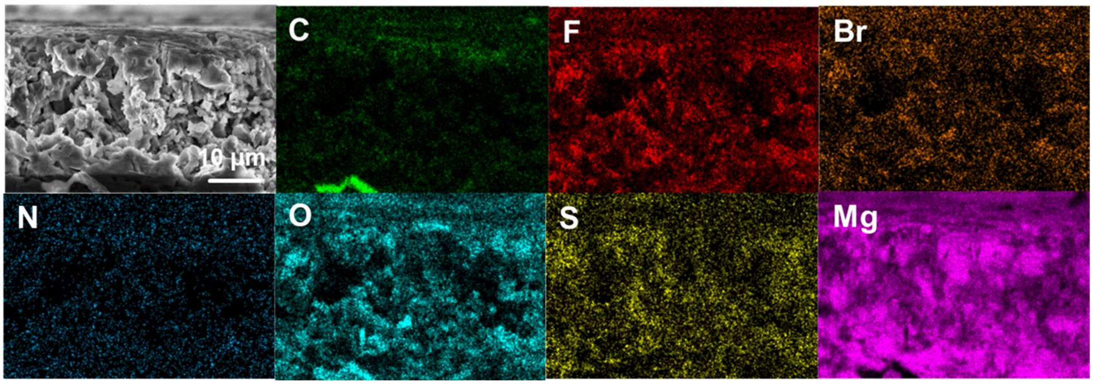

Figure S8. SEM image and corresponding EDS element mapping of Mg electrode after stripping in MBG electrolyte.

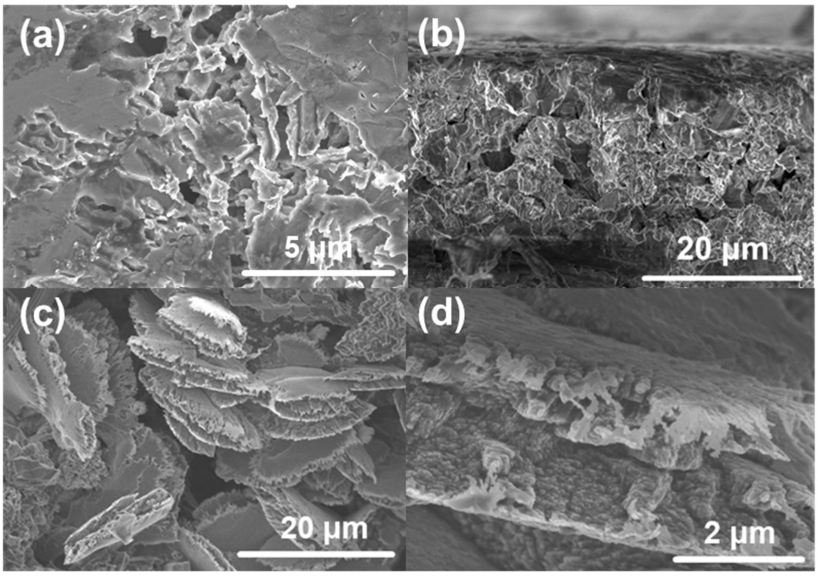

Figure S9. (a) Surface SEM image of Mg electrode after stripping at an areal capacity of 20 mAh cm^{-2}. (b) Cross-section SEM image of Mg electrode after stripping at an areal capacity of 20 mAh cm^{-2}. (c-d) Surface SEM images of Mg electrode after plating at an areal capacity of 20 mAh cm^{-2}.

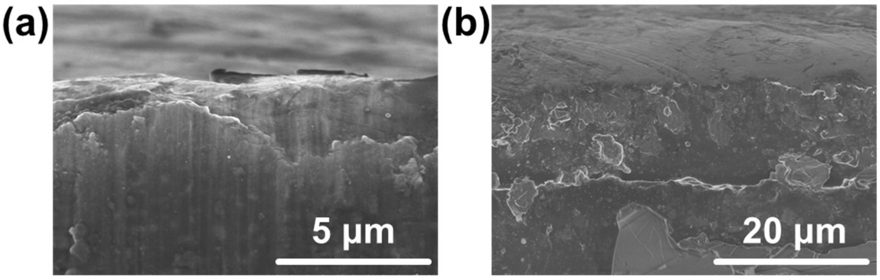

Figure S10. SEM images of Mg electrodes (a) before and (b) after plating in MBG electrolyte at an areal capacity of 20 mAh cm^{-2}.

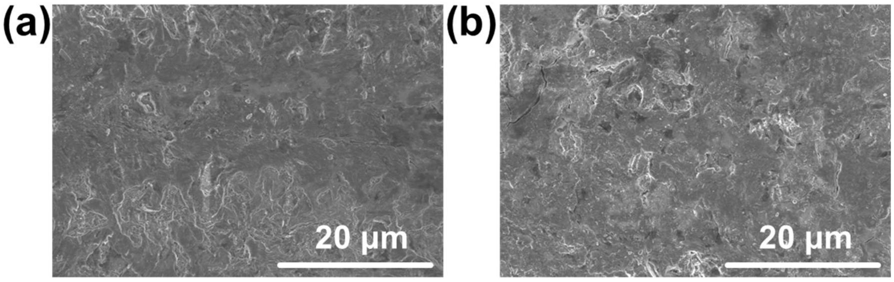

Figure S11. Top-view SEM images of Mg electrodes after (a) plating and (b) stripping after 200 cycles.

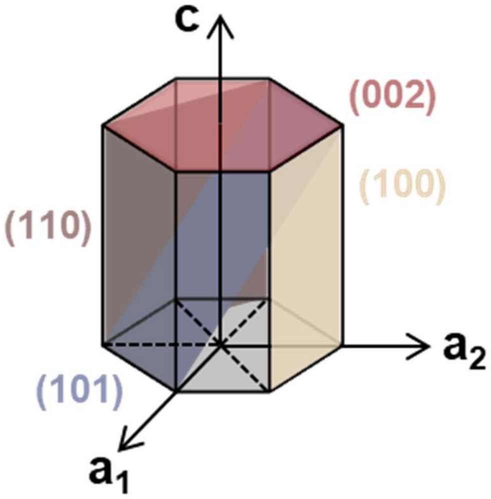

Figure S12. Schematic diagram of hcp-structure of Mg.

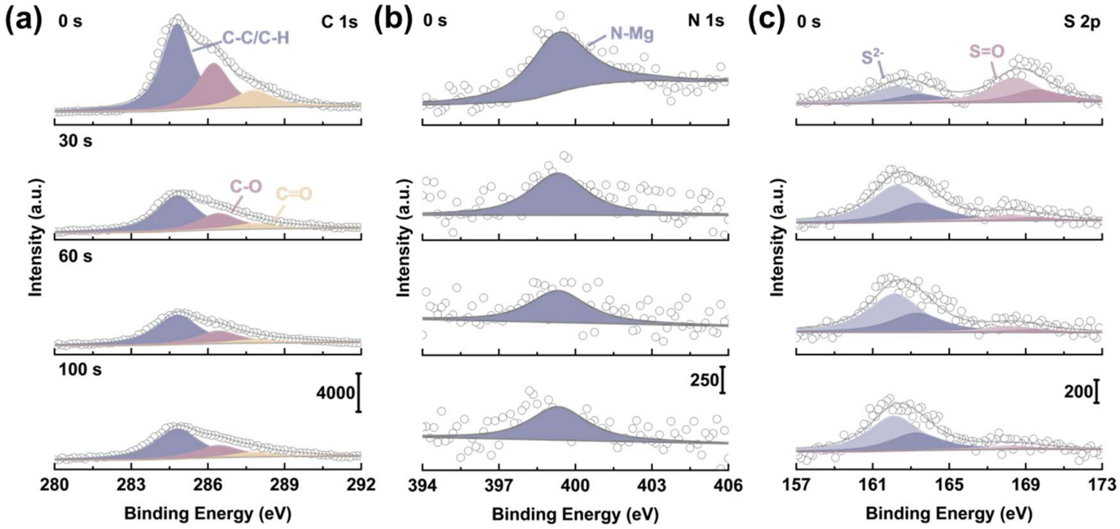

Figure S13. XPS spectra of Mg electrode surface after stripping with the signals of (a) C 1s, (b) N 1s and (c) S 2p.

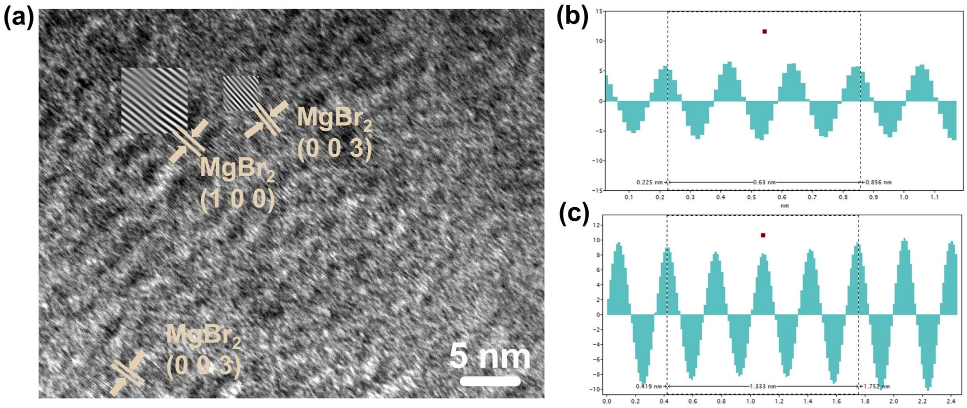

Figure S14. (a) High-resolution TEM image of ASEI and (b-c) measuring results of corresponding lattice distances from Mg electrode after 50th cycle at 0.5 mA cm^{-2}. Since the high-resolution imaging on vulnerable ASEI products is still very challenging in view of their poor crystallinity and potential instability (sensitivity) under electron-beam irradiation, we have to shorten the exposure time under electron-beam in order to grasp the accurate information of crystalline products in ASEI. For this sample, the HRTEM regions are difficult to be settled with time and therefore we have to take a picture under the condition of slowest region migration as soon as possible before the degradation of crystalline zones under irradiation. This operation somewhat causes the blurring of imaging, and fortunately the crystalline zones are kept in a maximum degree as clearly shown from the magnified lattice stripe patterns. Figures S14b and S14c show the measurement results correspond to the MgBr$_2$ (003) and (100) crystallographic planes, respectively.

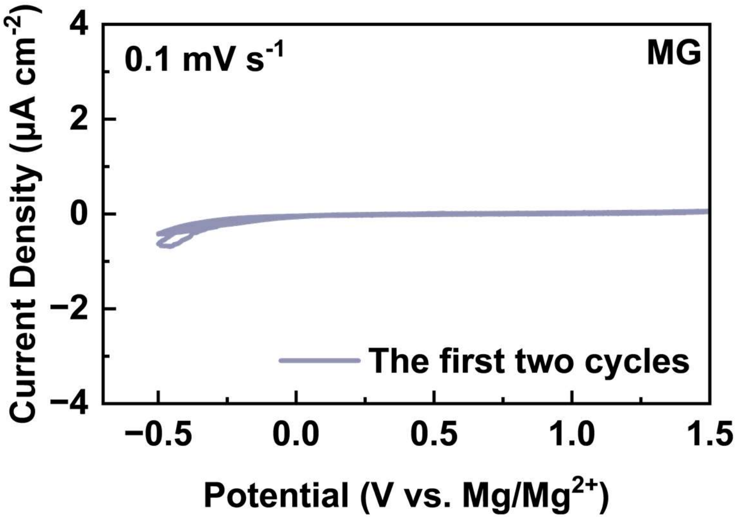

Figure S15. CV curves of c-Al||Mg asymmetric cell in MG electrolyte at 0.1 mV s^{-1}.

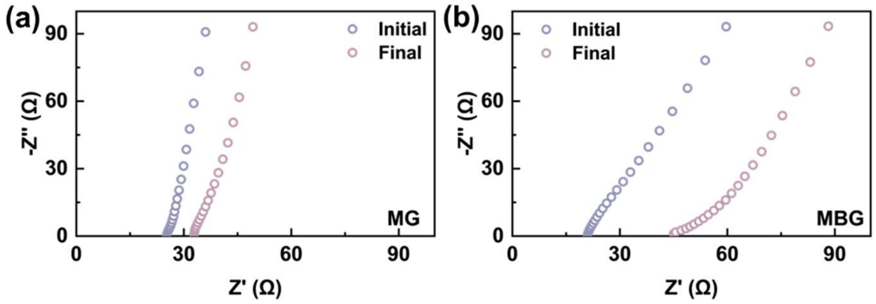

Figure S16. Impedance spectra of symmetric cells in (a) MG and (b) MBG electrolytes before and after polarization.

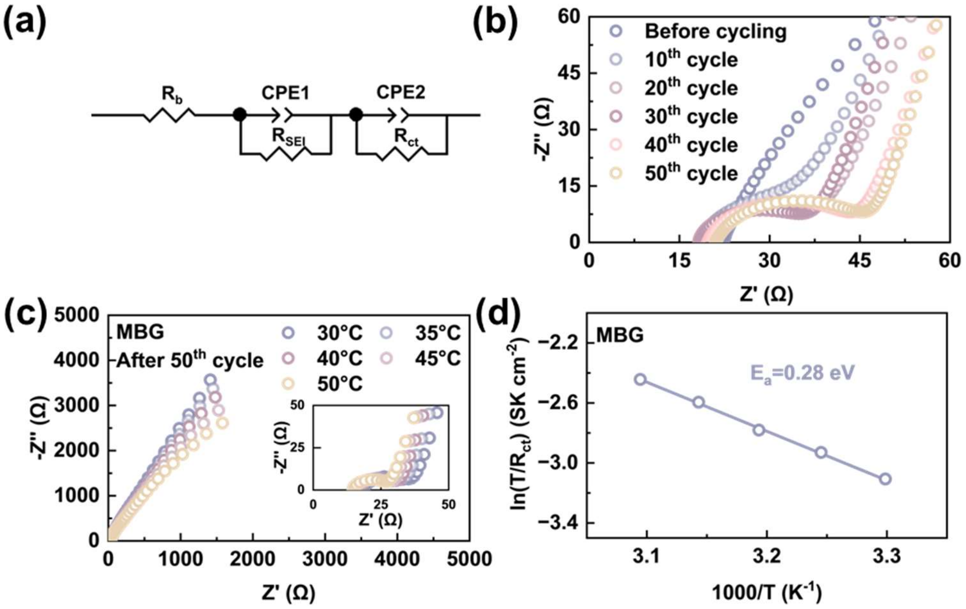

Figure S17. (a) Equivalent circuit model for fitting Nyquist plots. (b) EIS of Mg||Mg symmetric cell in MBG electrolyte at different cycling stages. (c) EIS of Mg||Mg symmetric cell in MBG electrolyte after 50 cycles at different temperatures. (d) Arrhenius plots of charge transfer resistances for MBG electrolyte system after 50 cycles to calculate activation energy.

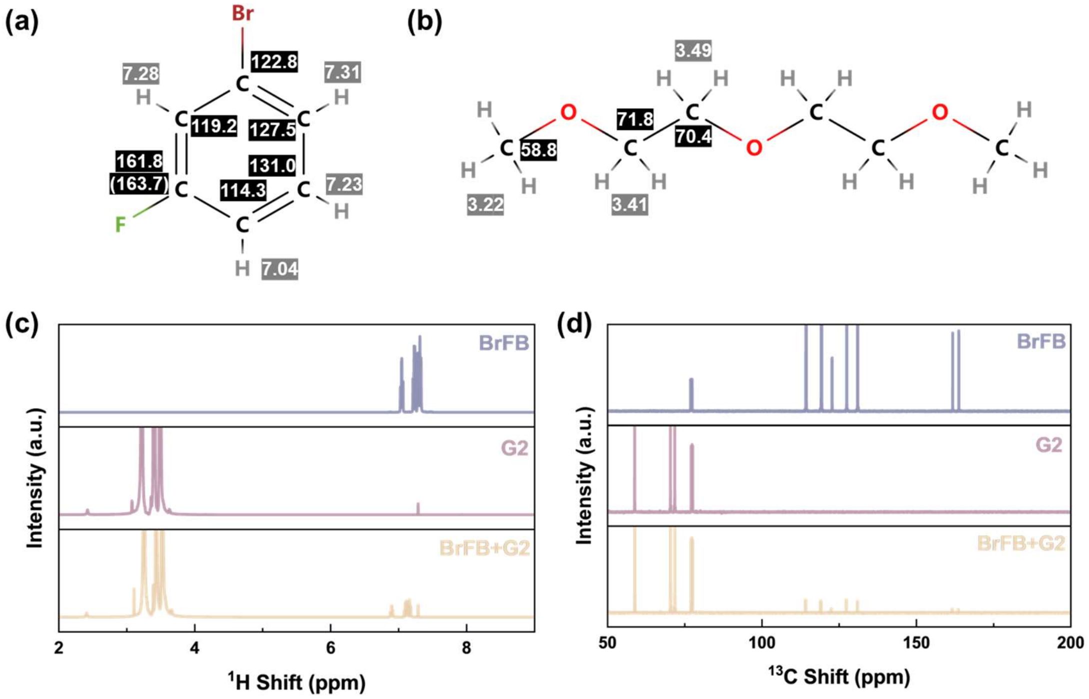

Figure S18. Molecular structures of (a) BrFB and (b) G2 with chemical shift values at different atom sites. (c) ^{1}H and (d) ^{13}C NMR spectra of BrFB, G2 and BrFB+G2 electrolytes.

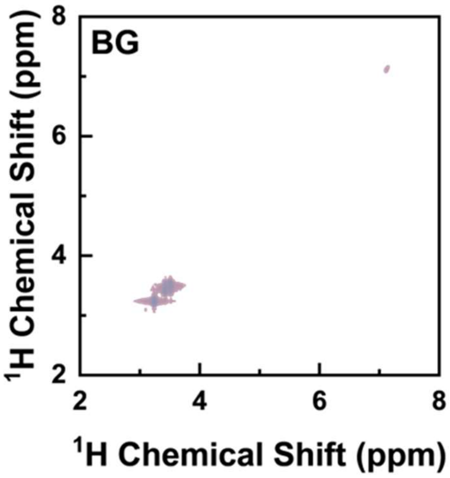

Figure S19. ^{1}H-^{1}H HOESY of BG electrolyte.

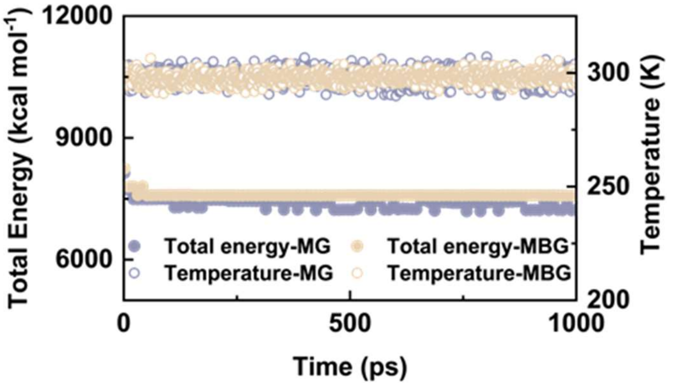

Figure S20. Evolution illustration of total energies and temperatures of MG and MBG electrolyte systems.

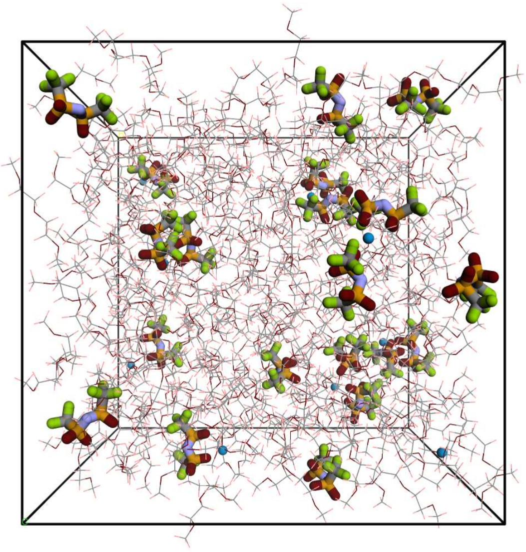

Figure S21. Snapshot of solvation structure in MG electrolyte calculated by MD.

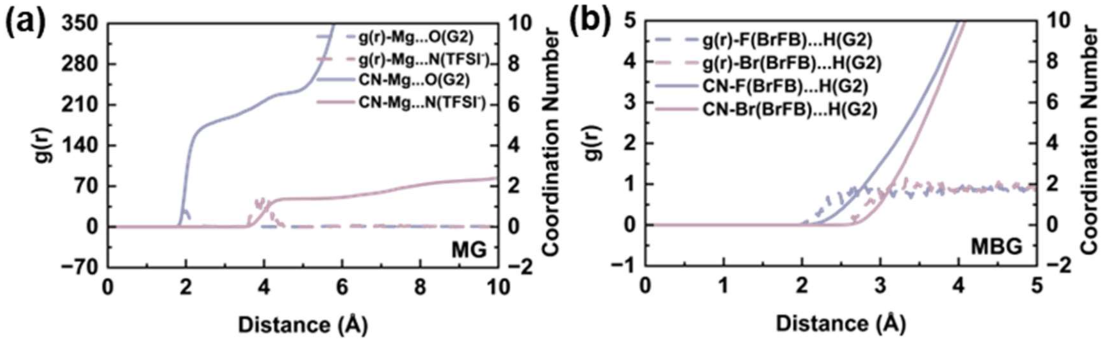

Figure S22. Radial distribution functions and coordination numbers of different interactions in (a) MG and (b) MBG electrolytes.

Table S1. Comparison of electrolyte additive strategy and corresponding cycling performance of our Mg||Mg symmetric cells with previously reported modified electrolytes.

Electrolyte	Additive	Current density (mA cm^{-2})	Areal capacity (mAh cm^{-2})	T e	Cycling life (h)	Overpotential (mV)	Ref.
$Mg(OTf)_2$-DME	$MgCl_2$	0.5	1	RT	500	300	[6]
$Mg(OTf)_2$-DME	TBACl	0.5	0.5	RT	600	290	[7]
$Mg(HMDS)_2$-DME	$TBABH_4$+$MgBr_2$	0.5	0.5	RT	2000	410	[8]
$Mg[B(hfip)_4]_2$-DME	$Bi(OTf)_3$	1	0.5	RT	500	210	[9]
$Mg(TFSI)_2$-DME	$GeCl_4$	0.02	0.005	RT	1000	250	[10]
$Mg(OTf)_2$-DME	$InCl_3$	1	1	RT	340	200	[11]
$Mg(OTf)_2$-DME-G2	2-methoxyethanamine	0.1	0.05	RT	1000	100	[12]
$Mg(OTf)_2$-G2	2-methoxyethanamine	0.5	0.25	RT	5000	100	[13]
$Mg(TFSI)_2$-DME	Aniline	0.1	0.025	RT	150	150	[14]
$Mg(TFSI)_2$-DME	3-methoxypropylamine	0.1	0.1	RT	360	50	[15]
$Mg(TFSI)_2$-DME	TMP	0.1	0.025	RT	300	1000	[16]
$Mg(OTf)_2$-DME	1-chloropropane	5	5	RT	430	500	[17]
$Mg(HMDS)_2$-$Mg(OTf)_2$-DME	TBAOTf	0.5	0.5	RT	450	2000	[18]
$Mg(OTf)_2$-PC	Water	0.01	0.005	RT	800	800	[19]
$Mg(TFSI)_2$-DME	5,10,15,20-tetraphenylporphyrin	0.01	0.005	RT	500	800	[20]

Mg(TFSI)$_2$-DME	ethylenediamine dihydrochloride	0.1	0.1	RT	1200	2200	[21]
Mg(TFSI)$_2$-G2	3-bromofluorobenzene	0.1	0.05	RT	7000	190	**This work**
		0.1	5	RT	1100	400	
		0.5	30	RT	280	500	
		0.5	0.1	-20	600	1000	

Table S2. Element contents from EDS of Mg electrode after cycling in MBG electrolyte.

Element	**Line kinds**	**wt%**	**wt% Sigma**	**Atomic percent**
N	K	0.91	0.16	1.51
O	K	12.58	0.09	18.16
F	K	6.96	0.07	8.46
Mg	K	71.92	0.17	68.30
S	K	3.17	0.05	2.28
Br	L	4.45	0.10	1.29
Total:		100.00		100.00

References

[1] C. Du, Y. Zhu, Z. Wang, L. Wang, W. Younas, X. Ma, C. Cao, *ACS Appl. Mater. Interfaces* **2020**, *12*, 35035.

[2] J. D. Patterson, *Ann. Nucl. Energy* **1989**, *16*, 611.

[3] J. P. Perdew, K. Burke, M. Ernzerhof, *Phys. Rev. Lett.* **1996**, *77*, 3865.

[4] C. Lee, W. Yang, R. G. Parr, *Physical Review B* **1988**, *37*, 785.

[5] G. Henkelman, B. P. Uberuaga, H. Jónsson, *J. Chem. Phys.* **2000**, *113*, 9901.

[6] D.-T. Nguyen, A. Y. S. Eng, M.-F. Ng, V. Kumar, Z. Sofer, A. D. Handoko, G. S. Subramanian, Z. W. Seh, *Cell Rep. Phys. Sci.* **2020**, *1*, 100265.

[7] D.-T. Nguyen, A. Y. S. Eng, R. Horia, Z. Sofer, A. D. Handoko, M.-F. Ng, Z. W. Seh, *Energy Storage Mater.* **2022**, *45*, 1120.

[8] D. Chinnadurai, W. Y. Lieu, S. Kumar, G. Yang, Y. Li, Z. W. Seh, *Nano Lett.* **2023**, *23*, 1564.

[9] Z. Meng, Z. Li, L. Wang, T. Diemant, D. Bosubabu, Y. Tang, R. Berthelot, Z. Zhao-Karger, M. Fichtner, *ACS Appl. Mater. Interfaces* **2021**, *13*, 37044.

[10] J. Zhang, X. Guan, R. Lv, D. Wang, P. Liu, J. Luo, *Energy Storage Mater.* **2020**, *26*, 408.

[11] G. Yang, Y. Li, C. Zhang, J. Wang, Y. Bai, C. Y. J. Lim, M.-F. Ng, Z. Chang, S. Kumar, Z. Sofer, W. Liu, Z. W. Seh, *Nano Lett.* **2022**, *22*, 9138.

[12] Y. Du, Y. Chen, S. Tan, J. Chen, X. Huang, L. Cui, J. Long, Z. Wang, X. Yao, B. Shang, G. Huang, X. Zhou, L. Li, J. Wang, F. Pan, *Energy Storage Mater.* **2023**, *62*, 102939.

[13] D. Zhang, Y. Wang, Y. Yang, Y. Zhang, Y. Zhao, M. Pan, Y. Sun, S. Chen, X. Liu, J. Wang, Y. NuLi, *Adv. Energy Mater.* **2023**, *13*, 2301795.

[14] Y. Liu, W. Zhao, Z. Pan, Z. Fan, M. Zhang, X. Zhao, J. Chen, X. Yang, *Angew. Chem. Int. Ed.* **2023**, *62*, e202302617.

[15] F. Wang, H. Hua, D. Wu, J. Li, Y. Xu, X. Nie, Y. Zhuang, J. Zeng, J. Zhao, *ACS Energy Lett.* **2023**, *8*, 780.

[16] W. Zhao, Z. Pan, Y. Zhang, Y. Liu, H. Dou, Y. Shi, Z. Zuo, B. Zhang, J. Chen, X. Zhao, X. Yang, *Angew. Chem. Int. Ed.* **2022**, *61*, e202205187.

[17] G. Yang, Y. Li, J. Wang, Y. Lum, C. Y. J. Lim, M.-F. Ng, C. Zhang, Z. Chang, Z. Zhang, A. D. Handoko, T. Ghosh, S. Li, Z. Sofer, W. Liu, Y. Yao, Z. W. Seh, *Energy Environ. Sci.* **2024**, *17*, 1141.

[18] D. Chinnadurai, Y. Li, C. Zhang, G. Yang, W. Y. Lieu, S. Kumar, Z. Xing, W. Liu, Z. W. Seh, *Nano Lett.* **2023**, *23*, 11233.

[19] G. Li, Y. Li, M. Lei, K. Chen, C. Li, *Small* **2024**, *20*, 2405568.

[20] Y. Zhuang, J. Wu, H. Hua, F. Wang, D. Wu, Y. Xu, J. Zeng, J. Zhao, *Chem. Eng. J.* **2024**, *481*, 148170.

[21] W. Wang, S. Ju, H. Zhang, X. Zhou, X. Yu, *Energy Storage Mater.* **2024**, *70*, 103493.